Advances in Nano Research, *Vol. 17, No. 6 (2024) 533-546*
https://doi.org/10.12989/anr.2024.17.6.533

The natural frequency analysis of FG-GNPR nanoplates under different boundary conditions

Adel Lakel[1], Lazreg Hadji*[1,2], Mehmet Avcar[3], Hassen Ait Atmane[4] and Royal Madan[5]

[1]*Laboratory of Geomatics and Sustainable Development, University of Tiaret, Algeria*
[2]*Suleyman Demirel University, Isparta, 32260, Turkiye*
[3]*Suleyman Demirel University, Department of Civil Engineering, Isparta, 32260, Turkiye*
[4]*Laboratory of Structures, Geotechnics and Risks, Department of Civil Engineering, Hassiba Benbouali University of Chlef, Chlef, Algeria*
[5]*Department of Mechanical Engineering, Graphic Era (Deemed to be University) Dehradun- 248002, India*

(*Received July 29, 2024, Revised November 6, 2024, Accepted November 7, 2024*)

Abstract. Because of their remarkable mechanical qualities, nano-composites—components that are 100 nanometers or smaller—have started to be used in modern engineering. Among these are graphene nanoplatelets (GNPs), which offer a number of advantages over other nanomaterials, including low gas permeability, thermal conductivity, and electrical conductivity. The present study presents natural frequency analysis of functionally graded graphene nanoplatelet reinforced (FG-GNPR) nanoplates. For this context, a refined four-variable plate theory (RPT) is utilized considering several boundary conditions. Eringen's nonlocal elasticity theory is employed to take account of the size-dependent effect of nanoplates. The distributions of GNPs in the polymer matrix are considered to be uniform and non-uniform patterns. Hamilton's principle is employed to solve the governing equations of FG-GNPR nanoplate. The obtained results are then validated with benchmark reulsts of available in the literature. Comprehensive parametrical investigations are carried out, and the effects of nonlocal parameter, weight fraction, and the boundary conditions on the free vibration response of FG-GNPR polymer composite nanoplates are examined in detail. For design engineers, the study offers insightful information on how various factors and boundary conditions affect the natural frequency of plates.

Keywords: boundary condition; composite nanoplates; graphene nanoplatelet; free vibration; Hamilton's principle; reinforcement

1. Introduction

Functionally graded materials (FGMs) are advanced composite materials whose properties vary gradually through directions. The change in the properties is a result of a change in composition, microstructure gradient, or porosity (Avcar 2019, Madan and Bhowmick 2020, Sankar 2001). The fabrication processes of FGMs involve gas-based, liquid-based, and solid-based methods (Bykov 2012). Liquid-based methods like centrifugal casting are suitable for creating axisymmetric objects by dispersing reinforcement in a molten metal pool via rotation (Chen *et al*. 2001). The solid-based methods like powder metallurgy and additive manufacturing are preferred for complex geometries (Madan and Bhowmick 2022). However, layer-based methods may suffer from stress concentration at interfaces, leading to delamination (Nakamura *et al*. 2000, Norio *et al*. 1992). Because additive manufacturing can produce several thin layers, it has the benefit of preventing delamination. (Abdalla *et al*. 2021, Benoit *et al*. 2021). Centrifugal casting, while offering continuous distribution of graded material, lacks control over composition changes, which is achievable in powder metallurgy. Factors like pouring temperature and rotation speed affect its efficacy (Akinwamide *et al*. 2020).

Free vibration analysis using the Iso-Geometric Approach (IGA), a spline-based FEM, is performed, and its results are compared with FEM, the Rayleigh-Ritz method, and experimental data for benchmark tests on block and cylinder models. Convergence rate, accuracy, and computational time are compared between IGA and FEM, considering spline order and parameterization effects (Kolman *et al*. 2015). Also, an iso-geometric method offers the advantage of accurately representing mesh geometry through a connection between CAD and NURBS shape functions (Cottrell *et al*. 2006, Hughes *et al*. 2005). The dynamic analysis of the FG structures has been carried out by employing several methods such as the pseudo-spectral method (Jalali and Heshmati, 2020), differential quadrature method (Lal and Saini 2020, Elnaz Zare *et al*. 2024), dynamic model with the dynamic stiffening effect (Li and Zhang 2016), non-uniform rational B-spline (Lieu *et al*. 2019). Finite element method (Liu and Lee 2000), new hyperbolic shear deformation theory (Mahi *et al*. 2015), Galerkin's approach (Menasria *et al*. 2020), simple shear deformation theory (Hadji and Avcar 2021, Ebrahimi and Jafari 2017, Taibi *et al*. 2015), are to name a few. Cornacchia *et al*. (2019) presented an analytical solution for the linear vibration and buckling of cross- and angle-ply nanoplates utilizing strain gradient theory. Luciano *et al*. (2020) examined the free flexural vibration of nanobeams with non-classical boundary conditions using the stress-driven nonlocal model.

*Corresponding author, Professor,
E-mail: lazreg.hadji@univ-tiaret.dz

ISSN: 2287-237X (Print), 2287-2388 (Online)

Recently, new research has been developed on the dynamics of functionally graded material (FGM) beams resting on two- and three-parameter foundation models, with and without variable Winkler coefficient. (Ait Atmane *et al*. 2010, 2015, 2021, Hadji *et al*. 2022, Avcar *et al*. 2022, Nebab *et al*. 2023, Djilali Djebbour *et al*. 2024). Several studies consider the multidirectional variation of material properties in FGM and has been incorporated into new dynamic and stability studies (Hadji *et al*. 2024a, Zouatnia *et al*. 2024, Dedbaghi *et al*. 2024, Dahmane *et al*. 2023). Hadji *et al*. (2024b) incorporated thermal buckling analysis of functionally graded plates using trigonometric shear deformation theory, accounting for temperature-dependent material properties.

Aluminium is preferred as a matrix material due to its high strength-to-weight ratio (Aruri *et al*. 2013, Al-Shafaie *et al*. 2021, Huang *et al*. 2022). Graphene, on the other hand, imparts superior mechanical, electrical, and thermal properties (Bisht *et al*. 2017, Tavakol *et al*. 2023, Mohd and Talha 2022). Manufacturing technology for Functionally Graded Graphene Nanoplate Reinforced (FG-GNPR) composites involves advanced techniques like powder metallurgy, additive manufacturing, and hot pressing to create materials with a gradual variation in properties across their thickness. FG-GNPR nanoplates are engineered to enhance mechanical, thermal, and electrical properties by leveraging the unique characteristics of graphene at nanoscale levels. These composites find applications in various fields, including aerospace, automotive, electronics, and biomedical industries. Their graded structure makes them ideal for components that require high strength-to-weight ratios, wear resistance, and efficient thermal management, such as turbine blades, heat exchangers, and medical implants. For even and uneven porosity distributions of graphene platelets (GNP), free vibration analyses are performed using the differential quadrature method (Gao *et al*. 2018, Li *et al*. 2021). Notably, increasing the GNP weight fraction parameter makes the plate stiffer, leading to an increase in non-dimensional fundamental frequencies (Cong and Duc 2023). Apart from these, several methods have been employed by many researchers to study the dynamic behaviours of FG-GNPR structures, such as cylindrical shell problem using Navier's method (Abedini Baghbadorani and Kiani 2021), composite nano plate using two-variable sinusoidal shear deformation theory (Arefi *et al*. 2018), multilayer FG graphene nanoplatelets reinforced composite plates using the NURBS formulation (Thai *et al*. 2019), first-order shell theory and a semi-analytical approach (Mirjavadi *et al*. 2019, Twinkle and Pitchaimani 2021), finite element method (Muni Rami Reddy *et al*. 2018).

According to the literature mentioned above, no study to date has explored the impact of distinct graphene nano-platelet distributions on the mechanical properties and natural frequencies of nanoplates. Focusing on the free vibration of FG-GNPR nanoplates under different boundary conditions is a novel problem and helps in understanding their performance under various constraints. Therefore, in this study, a refined four-variable plate theory (RPT) is employed to analyze the free vibration characteristics of FG

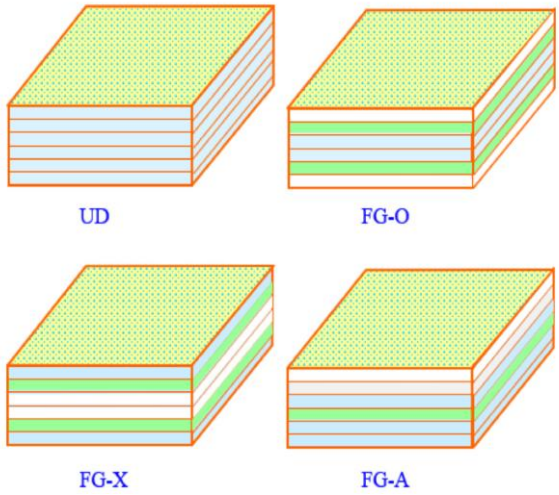

Fig. 1 Four GNP distribution patterns in multilayer GPL/ polymer nano-composite plates

FG-GNPR nanoplates. The investigation focused on varying boundary conditions: simply supported on all edges (SSSS), clamped on all edges (CCCC), clamped-simply supported-clamped-simply supported (CSCS), and free-clamped-free-clamped (FCFC), while considering different parameters a/h and μ. Graphene nanoplatelets are assumed to be distributed in four distinct patterns: uniformly distributed (UD), concentrated maximally at the middle (FG-O), concentrated at the top and bottom surfaces (FG-X), and incrementally increasing from bottom to top (FG-A). These distributions are examined to determine their impact on the natural frequencies of the FG-GNPR nanoplates. The primary objective is to identify the most effective graphene distribution pattern that enhances the structural stability and performance of FG-GNPR nanoplates. By comparing the obtained natural frequencies for these different distributions, the study aimed to pinpoint which reinforcement strategy optimally improves the overall mechanical behaviour of FG-GNPR nanoplates.

2. Problem formulation

A multilayer GPLs/polymer nano-composite nanoplate (length a, thickness h) is considered. The nanoplate, which has N_L layers, is reinforced by GNPs in the polymer matrix of each layer. The effects of distributions of GNPs on free vibration responses of the FG-GNPR nanoplates under various boundary conditions are examined in four patterns of distributions of GNPs, as indicated in Fig. 1. (Song *et al*. 2017).

$$g_{GNP}^{(k)} = \begin{cases} g_{GNP}^{*} & \text{UD (Patern 1)} \\ \dfrac{4g_{GNP}^{*}\left(\frac{N_L+1}{2} - \left|k - \frac{N_L+1}{2}\right|\right)}{2+N_L} & \text{FG} - \text{O (Patern 2)} \\ \dfrac{4g_{GNP}^{*}\left(\frac{1}{2} + \left|k - \frac{N_L+1}{2}\right|\right)}{2+N_L} & \text{FG} - \text{X (Patern 3)} \\ \dfrac{4kg_{GNP}^{*}}{N_L+1} & \text{FG} - \text{A (Patern 4)} \end{cases} \quad (1)$$

where g^*_{GNP} is the total GNPs weight fraction, k= 1, 2, . . ., N_L. Among, the pattern 1 (UD) is a special case where the GNPs are uniformly distribution across all layers. In pattern 2 (FG-O), the mid-plane of the nanoplate is rich with GNPs, while in pattern 3 (FG-X), the bottom and the top of the nanoplate are GPLs rich. For pattern 4 (FG-A), the GPL weight fraction increases from the bottom layer to the top layer.

2.1 Material properties

Halpin-Tsai model is used to estimate Young's modulus of the nanoplate, wherein the GNPs are assumed to be rectangular solid fillers in a polymer matrix. Young's modulus can be formulated as (Kitipornchai *et al*. 2017, Affdl and Kardos 1976, Yang *et al*. 2017):

$$E_c^{(k)} = \frac{3}{8}\frac{1+\xi_L\eta_L V_{GNP}^{(k)}}{1-\eta_L V_{GNP}^{(k)}}\times E_M + \frac{5}{8}\frac{1+\xi_w\eta_w V_{GNP}^{(k)}}{1-\eta_w V_{GNP}^{(k)}}\times E_M \tag{2}$$

where $V_{GNP}^{(k)}$ is the volume fraction of the GNPs, E_M and E_{GNP} refers to Young's modulus of the polymer matrix and GNPs, respectively.

Two additional parameters η_L and η_w are introduced as follows:

$$\eta_L = \frac{(E_{GNP}/E_M)-1}{(E_{GNP}/E_M)+\xi_L},\ \eta_w = \frac{(E_{GNP}/E_M)-1}{(E_{GNP}/E_M)+\xi_w} \tag{3}$$

where ξ_L and ξ_w are depend on the geometry and size of the GNP nanofillers, as follows:

$$\xi_L = 2(l_{GNP}/h_{GNP})\ ,\quad \xi_W = 2(w_{GNP}/h_{GNP}) \tag{4}$$

and l_{GNP}, w_{GNP}, h_{GNP} refer to the average length, width, and thickness of the GNPs, respectively. In addition, the volume fraction $V_{GNP}^{(k)}$ in Eq. (2) is defined as follows:

$$V_{GNP}^{(k)} = \frac{g_{GNP}^{(k)}}{g_{GNP}^{(k)} + (\rho_{GNP}/\rho_M)\left(1-g_{GNP}^{(k)}\right)} \tag{5}$$

where $g_{GNP}^{(k)}$ is the weight fraction for the k-layer of GNPs. Moreover, ρ_{GNP} and ρ_M refers to the density of GNPs and polymers, respectively.

The effective density and Poisson's ratio for the FG-GNPR nanoplate for the k-layer is defined, according to the rule of mixtures, as follows:

$$\begin{aligned}\rho_c^{(k)} &= \rho_{GNP}V_{GNP}^{(k)} + \rho_M\left(1-V_{GNP}^{(k)}\right)\\ \nu_c^{(k)} &= \nu_{GNP}V_{GNP}^{(k)} + \nu_M\left(1-V_{GNP}^{(k)}\right)\end{aligned} \tag{6}$$

ν_{GNP}, ν_M being the Poisson's ratios of GNPs and polymer matrix, respectively.

2.2 Kinematic, strain and stress relations

The assumed field of displacements can be defined by the subsequent equation (Shimpi 2002):

$$\begin{aligned}u(x,y,z,t) &= u_0(x,y,t) - z\frac{\partial w_b}{\partial x} - f(z)\frac{\partial w_s}{\partial x}\\ v(x,y,z,t) &= v_0(x,y,t) - z\frac{\partial w_b}{\partial y} - f(z)\frac{\partial w_s}{\partial y}\end{aligned} \tag{7}$$

$$w(x,y,z,t) = w_b(x,y,t) + w_s(x,y,t)$$

in which t represents the time, u_0 and v_0 signify the displacement functions of the middle surfaces of the FG GNPR. Also, $f(z)$ refers to the variation of the transverse shear strain along with the nanoplate thickness:

$$f(z) = z\left[1+\frac{3\pi}{2}sech\left(\frac{1}{2}\right)^2\right] - \frac{3\pi}{2}h\,tanh\left(\frac{z}{h}\right) \tag{8}$$

The nonzero strains relating to the displacement field are:

$$\begin{aligned}\begin{Bmatrix}\varepsilon_x\\ \varepsilon_y\\ \gamma_{xy}\end{Bmatrix} &= \begin{Bmatrix}\varepsilon_x^0\\ \varepsilon_y^0\\ \gamma_{xy}^0\end{Bmatrix} + z\begin{Bmatrix}k_x^b\\ k_y^b\\ k_{xy}^b\end{Bmatrix} + f(z)\begin{Bmatrix}k_x^s\\ k_y^s\\ k_{xy}^s\end{Bmatrix}\\ \begin{Bmatrix}\gamma_{yz}\\ \gamma_{xz}\end{Bmatrix} &= g(z)\begin{Bmatrix}\gamma_{yz}^s\\ \gamma_{xz}^s\end{Bmatrix}\end{aligned} \tag{9}$$

where

$$\begin{Bmatrix}\varepsilon_x^0\\ \varepsilon_y^0\\ \gamma_{xy}^0\end{Bmatrix} = \begin{Bmatrix}\frac{\partial u_0}{\partial x}\\ \frac{\partial v_0}{\partial x}\\ \frac{\partial u_0}{\partial y}+\frac{\partial v_0}{\partial x}\end{Bmatrix},\ \begin{Bmatrix}k_x^b\\ k_y^b\\ k_{xy}^b\end{Bmatrix} = \begin{Bmatrix}-\frac{\partial^2 w_b}{\partial x^2}\\ -\frac{\partial^2 w_b}{\partial y^2}\\ -2\frac{\partial^2 w_b}{\partial x\partial y}\end{Bmatrix},$$
$$\begin{Bmatrix}k_x^s\\ k_y^s\\ k_{xy}^s\end{Bmatrix} = \begin{Bmatrix}-\frac{\partial^2 w_s}{\partial x^2}\\ -\frac{\partial^2 w_s}{\partial y^2}\\ -2\frac{\partial^2 w_s}{\partial x\partial y}\end{Bmatrix},\ \begin{Bmatrix}\gamma_{yz}^s\\ \gamma_{xz}^s\end{Bmatrix} = g(z)\begin{Bmatrix}\frac{\partial w_s}{\partial y}\\ \frac{\partial w_s}{\partial x}\end{Bmatrix} \tag{10a}$$

then

$$g(z) = 1 - \frac{df(z)}{dz} \tag{10b}$$

The nonlocal stress-strain relations for the kth-layer are expressed as (Arefi and Zenkour 2016):

$$\left(1-\mu^2\nabla^2\right)\begin{Bmatrix}\sigma_x\\ \sigma_y\\ \tau_{yz}\\ \tau_{xz}\\ \tau_{xy}\end{Bmatrix}^{(k)} = \begin{bmatrix}Q_{11}^{(k)} & Q_{12}^{(k)} & 0 & 0 & 0\\ Q_{21}^{(k)} & Q_{22}^{(k)} & 0 & 0 & 0\\ 0 & 0 & Q_{44}^{(k)} & 0 & 0\\ 0 & 0 & 0 & Q_{55}^{(k)} & 0\\ 0 & 0 & 0 & 0 & Q_{66}^{(k)}\end{bmatrix}\begin{Bmatrix}\varepsilon_x\\ \varepsilon_y\\ \gamma_{yz}\\ \gamma_{xz}\\ \gamma_{xy}\end{Bmatrix}^{(k)} \tag{11}$$

where μ is the nonlocal parameter, ∇^2 is the Laplacian and Q_{ij} represents the stiffness coefficients in terms of Young's modulus and Poisson's ratio, defined as

$$\begin{aligned}Q_{11}{}^{(k)} = Q_{22}{}^{(k)} &= \frac{E_c^{(k)}}{1-\left(\nu_c^{(k)}\right)^2},\\ Q_{12}{}^{(k)} = Q_{21}{}^{(k)} &= \frac{\nu_c^{(k)}E_c^{(k)}}{1-\left(\nu_c^{(k)}\right)^2},\\ Q_{44}{}^{(k)} = Q_{55}{}^{(k)} = Q_{66}{}^{(k)} &\frac{E_c^{(k)}}{2\left(1+\nu_c^{(k)}\right)}\end{aligned} \tag{12}$$

Utilizing Hamilton's principle, the equations of motion could be found as follows:

$$0 = \int_0^t (\delta U - \delta T)\,dt \tag{13}$$

where δU and δT are the variations of strain and kinetic

energies, respectively.

The variation of strain energy can be specified as follows:

$$\begin{aligned}\delta U &= \int_V \left[\sigma_x \delta\,\varepsilon_x + \sigma_y \delta\,\varepsilon_y + \tau_{xy}\delta\,\gamma_{xy} + \tau_{yz}\delta\,\gamma_{yz} + \tau_{xz}\delta\,\gamma_{xz}\right] dV \\ &= \int_A \left[N_x \delta\,\varepsilon_x^0 + N_y \delta\,\varepsilon_y^0 + N_{xy}\delta\,\gamma_{xy}^0 + M_x^b \delta\,k_x^b + M_y^b \delta\,k_y^b + M_{xy}^b \delta\,k_{xy}^b + M_x^s \delta\,k_x^s + M_y^s \delta\,k_y^s + M_{xy}^s \delta\,k_{xy}^s + S_{yz}^s \delta\,\gamma_{yz}^s + S_{xz}^s \delta\,\gamma_{xz}^s\right] dA = 0\end{aligned} \tag{14}$$

here A is the upper surface of FG-GNPR nanoplate and the stress resultants N, M, and S can be described as follows

$$\left(N_i, M_i^b, M_i^s\right) = \int_{-h/2}^{h/2} (1, z, f)\sigma_i dz\,, (i = x, y, xy) \tag{15a}$$

$$\left(S_{xz}^s, S_{yz}^s\right) = \int_{-h/2}^{h/2} g\left(\tau_{xz}, \tau_{yz}\right) dz \tag{15b}$$

The variation of the kinetic energy can be specified as follows:

$$\begin{aligned}\delta T &= \int_{-\frac{h}{2}}^{\frac{h}{2}} \int_\Omega \left[\dot{u}\delta\,\dot{u} + \dot{v}\delta\,\dot{v} + \dot{w}\delta\,\dot{w}\right] \rho(z)\, d\Omega\, dz \\ &= \int_A \{I_0[\dot{u}_0\delta\dot{u}_0 + \dot{v}_0\delta\dot{v}_0 + (\dot{w}_b + \dot{w}_s)(\delta\dot{w}_b + \delta\dot{w}_s)] \\ &-I_1\left(\dot{u}_0\frac{\partial\delta\dot{w}_b}{\partial x} + \frac{\partial\dot{w}_b}{\partial x}\delta\,\dot{u}_0 + \dot{v}_0\frac{\partial\delta\dot{w}_b}{\partial y} + \frac{\partial\dot{w}_b}{\partial y}\delta\,\dot{v}_0\right) \\ &-I_2\left(\dot{u}_0\frac{\partial\delta\dot{w}_s}{\partial x} + \frac{\partial\dot{w}_s}{\partial x}\delta\,\dot{u}_0 + \dot{v}_0\frac{\partial\delta\dot{w}_s}{\partial y} + \frac{\partial\dot{w}_s}{\partial y}\delta\,\dot{v}_0\right) \\ &+J_1\left(\frac{\partial\dot{w}_b}{\partial x}\frac{\partial\delta\,\dot{w}_b}{\partial x} + \frac{\partial\dot{w}_b}{\partial y}\frac{\partial\delta\,\dot{w}_b}{\partial y}\right) \\ &+K_2\left(\frac{\partial\dot{w}_s}{\partial x}\frac{\partial\delta\,\dot{w}_s}{\partial x} + \frac{\partial\dot{w}_s}{\partial y}\frac{\partial\delta\,\dot{w}_s}{\partial y}\right) \\ &+J_2\left(\begin{array}{l}\frac{\partial\dot{w}_b}{\partial x}\frac{\partial\delta\,\dot{w}_s}{\partial x} + \frac{\partial\dot{w}_s}{\partial x}\frac{\partial\delta\,\dot{w}_b}{\partial x} \\ +\frac{\partial\dot{w}_b}{\partial y}\frac{\partial\delta\,\dot{w}_s}{\partial y} + \frac{\partial\dot{w}_s}{\partial y}\frac{\partial\delta\,\dot{w}_b}{\partial y}\end{array}\right)\Bigg\}\, d\Omega\end{aligned} \tag{16}$$

here, the dot superscript demonstrates differentiation concerning the variable of time t, I_i, J_i, K_i terms define mass moment of inertias of FG-GNPR nanoplate as follows:

$$(I_0, I_1, I_2) = \int_{-h/2}^{h/2} (1, z, z^2)\rho(z)dz \tag{17a}$$

$$(J_1, J_2, K_2) = \int_{-h/2}^{h/2} (f, z\,f, f^2)\rho(z)dz \tag{17b}$$

Considering the Eqs. (14) and (16) in Eq. (13), and after some mathematical operations and simplification, the subsequent equations are found

$$\delta\,u_0\colon\quad \frac{\partial N_x}{\partial x} + \frac{\partial N_{xy}}{\partial y} = I_0\ddot{u}_0 - I_1\frac{\partial\ddot{w}_b}{\partial x} - J_1\frac{\partial\ddot{w}_s}{\partial x} \tag{18}$$

$$\begin{aligned}&\delta\,v_0\colon\quad \frac{\partial N_{xy}}{\partial x} + \frac{\partial N_y}{\partial y} = I_0\ddot{v}_0 - I_1\frac{\partial\ddot{w}_b}{\partial y} - J_1\frac{\partial\ddot{w}_s}{\partial y} \\ &\delta\,w_b\colon\quad \frac{\partial^2 M_x^b}{\partial x^2} + 2\frac{\partial^2 M_{xy}^b}{\partial x\partial y} + \frac{\partial^2 M_y^b}{\partial y^2} \\ &= I_0(\ddot{w}_b + \ddot{w}_s) + I_1\left(\frac{\partial\ddot{u}_0}{\partial x} + \frac{\partial\ddot{v}_0}{\partial y}\right) - I_2\nabla^2\ddot{w}_b - J_2\nabla^2\ddot{w}_s \\ &\delta\,w_s\colon\quad \frac{\partial^2 M_x^s}{\partial x^2} + 2\frac{\partial^2 M_{xy}^s}{\partial x\partial y} + \frac{\partial^2 M_y^s}{\partial y^2} + \frac{\partial S_{xz}^s}{\partial x} + \frac{\partial S_{yz}^s}{\partial y} \\ &= I_0(\ddot{w}_b + \ddot{w}_s) + J_1\left(\frac{\partial\ddot{u}_0}{\partial x} + \frac{\partial\ddot{v}_0}{\partial y}\right) - J_2\nabla^2\ddot{w}_b - K_2\nabla^2\ddot{w}_s\end{aligned}$$

Considering Eqs. (11) and (10) in Eq. (15) and after some mathematical operations, the stress resultants concerning generalized displacements (u_0, v_0, w_b, w_s) as follows:

$$\begin{aligned}&\begin{Bmatrix}N\\M^b\\M^s\end{Bmatrix} - \mu\left(\frac{\partial^2}{\partial x^2} + \frac{\partial^2}{\partial y^2}\right)\begin{Bmatrix}N\\M^b\\M^s\end{Bmatrix} = \begin{bmatrix}A & B & B^s\\ B & D & D^s\\ B^s & D^s & H^s\end{bmatrix}\begin{Bmatrix}\varepsilon\\k^b\\k^s\end{Bmatrix}, \\ &S - \mu\left(\frac{\partial^2 S}{\partial x^2} + \frac{\partial^2 S}{\partial y^2}\right) = A^s\gamma\end{aligned} \tag{19}$$

where

$$\begin{aligned}&N = \left\{N_x, N_y, N_{xy}\right\}^t, \\ &M^b = \left\{M_x^b, M_y^b, M_{xy}^b\right\}^t, \qquad M^s = \left\{M_x^s, M_y^s, M_{xy}^s\right\}^t\end{aligned} \tag{20a}$$

$$\begin{aligned}&\varepsilon = \left\{\varepsilon_x^0, \varepsilon_y^0, \gamma_{xy}^0\right\}^t, \\ &k^b = \left\{k_x^b, k_y^b, k_{xy}^b\right\}^t,\ k^s = \left\{k_x^s, k_y^s, k_{xy}^s\right\}^t\end{aligned} \tag{20b}$$

$$\begin{aligned}&A = \begin{bmatrix}A_{11} & A_{12} & 0\\ A_{12} & A_{22} & 0\\ 0 & 0 & A_{66}\end{bmatrix},\ B = \begin{bmatrix}B_{11} & B_{12} & 0\\ B_{12} & B_{22} & 0\\ 0 & 0 & B_{66}\end{bmatrix}, \\ &D = \begin{bmatrix}D_{11} & D_{12} & 0\\ D_{12} & D_{22} & 0\\ 0 & 0 & D_{66}\end{bmatrix}\end{aligned} \tag{20c}$$

$$\begin{aligned}&B^s = \begin{bmatrix}B_{11}^s & B_{12}^s & 0\\ B_{12}^s & B_{22}^s & 0\\ 0 & 0 & B_{66}^s\end{bmatrix},\ D^s = \begin{bmatrix}D_{11}^s & D_{12}^s & 0\\ D_{12}^s & D_{22}^s & 0\\ 0 & 0 & D_{66}^s\end{bmatrix}, \\ &H^s = \begin{bmatrix}H_{11}^s & H_{12}^s & 0\\ H_{12}^s & H_{22}^s & 0\\ 0 & 0 & H_{66}^s\end{bmatrix}\end{aligned} \tag{20d}$$

$$S = \left\{S_{xz}^s, S_{yz}^s\right\}^t,\ \gamma = \left\{\gamma_{xz}^0, \gamma_{yz}^0\right\}^t, A^s = \begin{bmatrix}A_{44}^s & 0\\ 0 & A_{55}^s\end{bmatrix} \tag{20e}$$

where the integration constant is expressed in terms of the mechanical properties along the thickness direction as

$$\left\{A_{ij}, B_{ij}, D_{ij}, B_{ij}^s, D_{ij}^s, H_{ij}^s\right\}\sum_{k=1}^{N_L}\int_{z_{(k)}}^{z_{(k+1)}} Q_{ij}^{(k)}\left\{1, z, z^2, f(z), zf(z), f^2(z)\right\}dz \tag{21a}$$

$$A_{44}^s = A_{55}^s = \sum_{k=1}^{N_L}\int_{z_{(k)}}^{z_{(k+1)}} Q_{44}^{(k)}\left[g(z)\right]^2 dz \tag{21b}$$

Considering Eq. (19) in Eq. (18), the following equation is found:

$$\begin{aligned}&A_{11}\frac{\partial^2 u_0}{\partial x^2}+A_{66}\frac{\partial^2 u0}{\partial y^2}+(A_{12}+A_{66})\frac{\partial^2 v}{\partial x\partial y}\\&-B_{11}\frac{\partial^3 w_b}{\partial x^3}-(B_{12}+2B_{66})\frac{\partial^3 w_b}{\partial x\partial y^2}\\&-B_{11}^s\frac{\partial^3 w_s}{\partial x^3}-(B_{12}^s+2B_{66}^s)\frac{\partial^3 w_s}{\partial x\partial y^2}\\&=(1-\mu\nabla^2)\left[I_0\ddot{u}_0-I_1\frac{\partial\ddot{w}_b}{\partial x}-J_1\frac{\partial\ddot{w}_s}{\partial x}\right]\end{aligned}\tag{22a}$$

$$\begin{aligned}&(A_{12}+A_{66})\frac{\partial^2 u_0}{\partial x\partial y}+A_{66}\frac{\partial^2 v_0}{\partial x^2}+A_{22}\frac{\partial^2 v_0}{\partial y^2}\\&-(B_{12}+2B_{66})\frac{\partial^3 w_b}{\partial x^2\partial y}-B_{22}\frac{\partial^3 w_b}{\partial y^3}\\&-B_{22}^s\frac{\partial^3 w_s}{\partial y^3}-(B_{12}^s+2B_{66}^s)\frac{\partial^3 w_s}{\partial x^2\partial y}\\&=(1-\mu\nabla^2)\left[I_0\ddot{v}_0-I_1\frac{\partial\ddot{w}_b}{\partial y}-J_1\frac{\partial\ddot{w}_s}{\partial y}\right]\end{aligned}\tag{22b}$$

$$\begin{aligned}&B_{11}\frac{\partial^3 u_0}{\partial x^3}+(B_{12}+2B_{66})\frac{\partial^3 u_0}{\partial x\partial y^2}\\&+(B_{12}+2B_{66})\frac{\partial^3 v_0}{\partial x^2\partial y}+B_{22}\frac{\partial^3 v_0}{\partial y^3}-D_{11}\frac{\partial^4 w_b}{\partial x^4}\\&-2(D_{12}+2D_{66})\frac{\partial^4 w_b}{\partial x^2\partial y^2}-D_{22}\frac{\partial^4 w_b}{\partial y^4}-D_{11}^s\frac{\partial^4 w_s}{\partial x^4}\\&-2(D_{12}^s+2D_{66}^s)\frac{\partial^4 w_s}{\partial x^2\partial y^2}-D_{22}^s\frac{\partial^4 w_s}{\partial y^4}\\&=(1-\mu\nabla^2)\begin{bmatrix}I_0(\ddot{w}_b+\ddot{w}_s)+I_1\left(\frac{\partial\ddot{u}_0}{\partial x}+\frac{\partial\ddot{v}_0}{\partial y}\right)\\-I_2\nabla^2\ddot{w}_b-J_2\nabla^2\ddot{w}_s\end{bmatrix}\end{aligned}\tag{22c}$$

$$\begin{aligned}&B_{11}^s\frac{\partial^3 u_0}{\partial x^3}+(B_{12}^s+2B_{66}^s)\frac{\partial^3 u_0}{\partial x\partial y^2}\\&+(B_{12}^s+2B_{66}^s)\frac{\partial^3 v_0}{\partial x^2\partial y}+B_{22}^s\frac{\partial^3 v_0}{\partial y^3}-D_{11}^s\frac{\partial^4 w_b}{\partial x^4}\\&-2(D_{12}^s+2D_{66}^s)\frac{\partial^4 w_b}{\partial x^2\partial y^2}-D_{22}^s\frac{\partial^4 w_b}{\partial y^4}\\&-H_{11}^s\frac{\partial^4 w_s}{\partial x^4}-2(H_{12}^s+2H_{66}^s)\frac{\partial^4 w_s}{\partial x^2\partial y^2}\\&-H_{22}^s\frac{\partial^4 w_s}{\partial y^4}+A_{55}^s\frac{\partial^2 w_s}{\partial x^2}+A_{44}^s\frac{\partial^2 w_s}{\partial y^2}\\&=(1-\mu\nabla^2)\begin{bmatrix}I_0(\ddot{w}_b+\ddot{w}_s)+J_1\left(\frac{\partial\ddot{u}_0}{\partial x}+\frac{\partial\ddot{v}_0}{\partial y}\right)\\-J_2\nabla^2\ddot{w}_b-K_2\nabla^2\ddot{w}_s\end{bmatrix}\end{aligned}\tag{22d}$$

3. The solution of the problem

In the present part, solutions for the free vibration of FG-GNPR nanoplate under four different boundary conditions are found. The boundary conditions of a random edge are defined as follows:

Clamped (C) edge boundary conditions

$$u_0=v_0=w_b=w_s=\frac{\partial w_b}{\partial x}=\frac{\partial w_s}{\partial x}=0 \text{ at } x=0,a \tag{23a}$$

$$u_0=v_0=w_b=w_s=\frac{\partial w_b}{\partial y}=\frac{\partial w_s}{\partial y}=0 \text{ at } y=0,b \tag{23b}$$

Simply supported (S) edge boundary conditions

$$N_x=v_0=w_b=w_s=M_x=0 \text{ at } x=0,a \tag{24a}$$

$$u_0=N_y=w_b=w_s=M_y=0 \text{ at } y=0,b \tag{24b}$$

Free (F) edge boundary conditions

$$N_x=N_{xy}=\frac{\partial M_x}{\partial x}+2\frac{\partial M_{xy}}{\partial y}=Q_x=M_x=0 \text{ at x=0, a} \tag{25a}$$

$$N_{xy}=N_y+2\frac{\partial M_{xy}}{\partial y}+\frac{\partial M_y}{\partial y}=Q_y=M_y=0 \text{ at y=0, b} \tag{25b}$$

The subsequent appropriate expressions are utilized for the related boundary conditions

$$\begin{Bmatrix}u\\v\\w_b\\w_s\end{Bmatrix}=\sum_{m=1}^{\infty}\sum_{n=1}^{\infty}\begin{Bmatrix}U_{mn}\frac{\partial X_m(x)}{\partial x}Y_n(y)e^{i\omega t}\\V_{mn}X_m(x)\frac{\partial X_n(y)}{\partial y}e^{i\omega t}\\W_{bmn}X_m(x)Y_n(y)e^{i\omega t}\\W_{smn}X_m(x)Y_n(y)e^{i\omega t}\end{Bmatrix} \tag{26}$$

where U_{mn}, V_{mn}, W_{bmn}, and W_{smn} identify the random parameters and $\omega=\omega_{mn}$ shows the eigenfrequency related to $(m,n)^{th}$eigenmode. The functions $X_m(x)$ and $Y_n(y)$are suggested by Sobhy (2013) to satisfy various boundary conditions in Eqs. (23) and (25) and signify the deflected surface of the nanoplate approximately. In Table 1, the admissible functions for the various boundary conditions are given, note that $\lambda=m\pi/a$ and $\mu=n\pi/b$.

Substituting the expression (26) into the Eqs. (22) and multiplying each eigenfunction with the corresponding equation and integrating throughout the solution domain, and after some mathematical operations, the following equation is found

$$\left(\begin{bmatrix}a_{11}&a_{12}&a_{13}&a_{14}\\a_{21}&a_{22}&a_{23}&a_{24}\\a_{31}&a_{32}&a_{33}&a_{34}\\a_{41}&a_{42}&a_{43}&a_{44}\end{bmatrix}-\omega^2\begin{bmatrix}m_{11}&m_{12}&m_{13}&m_{14}\\m_{21}&m_{22}&m_{23}&m_{24}\\m_{31}&m_{32}&m_{33}&m_{34}\\m_{41}&m_{42}&m_{43}&m_{44}\end{bmatrix}\right)\begin{Bmatrix}U_{mn}\\V_{mn}\\W_{bmn}\\W_{smn}\end{Bmatrix}=\begin{Bmatrix}0\\0\\0\\0\end{Bmatrix} \tag{27}$$

in which

$$\begin{aligned}&a_{11}=A_{11}\alpha_{12}+A_{66}\alpha_8, a_{12}=(A_{12}+A_{66})\alpha_8,\\&a_{13}=-B_{11}\alpha_{12}-(B_{12}+2B_{66})\alpha_8,\\&a_{14}=-(B_{12}^s+2B_{66}^s)\alpha_8-B_{11}^s\alpha_{12},\\&a_{21}=(A_{12}+A_{66})\alpha_{10},\\&a_{22}=A_{22}\alpha_4+A_{66}\alpha_{10},\\&a_{23}=-B_{22}\alpha_4-(B_{12}+2B_{66})\alpha_{10},\\&a_{24}=-(B_{12}^s+2B_{66})\alpha_{10}-B_{22}^s\alpha_4,\\&a_{31}=B_{11}\alpha_{13}+(B_{12}+2B_{66})\alpha_{11},\\&a_{32}=(B_{12}+2B_{66})\alpha_{11}+B_{22}\alpha_5,\\&a_{33}=-D_{11}\alpha_{13}-2(D_{12}+2D_{66})\alpha_{11}-D_{22}\alpha_5,\\&a_{34}=-D_{11}^s\alpha_{13}-2(D_{12}^s+2D_{66}^s)\alpha_{11}-D_{66}^s\alpha_5,\\&a_{41}=B_{11}^s\alpha_{13}+(B_{12}^s+2B_{66}^s)\alpha_{11},\\&a_{42}=(B_{12}^s+2B_{66}^s)\alpha_{11}+B_{22}^s\alpha_5,\\&a_{43}=-D_{11}^s\alpha_{13}-2(D_{12}^s+2D_{66}^s)\alpha_{11}-D_{22}^s\alpha_5,\\&a_{44}=-H_{11}^s\alpha_{13}-2(H_{12}^s+2H_{66}^s)\alpha_{11}-H_{22}^s\alpha_5\\&\qquad+A_{44}^s\alpha_9+A_{55}^s\alpha_3\end{aligned}\tag{28a}$$

And

Table 1 The admissible functions for different boundary conditions (Sobhy 2013)

Boundary Conditions	$x=0$	$y=0$	$x=a$	$y=b$	$X_m(x)$	$Y_n(y)$
SSSS	S	S	S	S	$sin(\lambda x)$	$sin(\mu x)$
CSCS	C	S	C	S	$sin^2(\lambda x)$	$sin(\mu x)$
CCCC	C	C	C	C	$sin^2(\lambda x)$	$sin^2(\mu x)$
FCFC	F	C	F	C	$cos^2(\lambda x)\,[sin^2(\lambda x)+1]$	$sin^2(\mu x)$

Table 2 The first two natural frequencies $\overline{\omega}=\omega h\sqrt{\rho_m/E_m}$ of the FG-GNPR plate

Mode	Theories	Pattern				
		Pure epoxy	UD	FG-O	FG-X	FG-A
1	(Sobhy 2013)	0.0584	0.1216	0.1020	0.1378	0.1118
	Reddy *et al*. 2018)	0.0588	0.1225	0.0912	0.1420	0.1080
	(Phung-Van *et al*. 2021)	0.0584	0.1216	0.1023	0.1366	0.1118
	Present	0.0584	0.12158	0.10230	0.13654	0.11181
2	(Sobhy 2013)	0.1391	0.2895	0.2456	0.3249	0.2673
	Reddy *et al*. 2018)	0.1412	0.2941	0.2246	0.3245	0.2589
	(Phung-Van *et al*. 2021)	0.1391	0.2895	0.2470	0.3189	0.2674
	Present	0.1391	0.28955	0.24703	0.31845	0.26736

Table 3 The first non-dimensional natural frequency $\overline{\omega}=\omega h\sqrt{\rho/G}$ of the isotropic square nsanoplate

a/h	Theories	μ					
		0	1	2	3	4	5
10	SSDT (Aghababaei and Reddy 2009)	0.0935	0.0854	0.0791	0.0741	0.0699	0.0663
	FSDT (Aghababaei and Reddy 2009)	0.0930	0.0850	0.0788	0.0737	0.0696	0.0660
	RPT (Phung-Van *et al*. 2021)	0.0930	0.0850	0.0788	0.0737	0.0695	0.0660
	Present	0.0930	0.0850	0.0788	0.0737	0.0695	0.0659
20	SSDT (Aghababaei and Reddy 2009)	0.0239	0.0218	0.0202	0.0189	0.0179	0.0170
	FSDT (Aghababaei and Reddy 2009)	0.0239	0.0218	0.0202	0.0189	0.0178	0.0169
	RPT (Phung-Van *et al*. 2021)	0.0239	0.0218	0.0202	0.0189	0.0178	0.0169
	Present	0.0239	0.0218	0.0202	0.0189	0.0178	0.0169

$$
\begin{aligned}
&m_{11}=-I_0[\alpha_6-\mu(\alpha_{12}+\alpha_8)],\ m_{12}=0,\\
&m_{13}=I_1[\alpha_6-\mu(\alpha_{12}+\alpha_8)],\\
&m_{14}=J_1[\alpha_6-\mu(\alpha_{12}+\alpha_8)],\\
&m_{21}=0, m_{22}=-I_0[\alpha_2-\mu(\alpha_{10}+\alpha_4)],\\
&m_{23}=I_1[\alpha_2-\mu(\alpha_{10}+\alpha_4)],\\
&m_{24}=J_1[\alpha_2-\mu(\alpha_{10}+\alpha_4)],\\
&m_{31}=-I_1[\alpha_9-\mu(\alpha_{13}+\alpha_{11})],\\
&m_{32}=-I_1\big[\big(\alpha_3-\mu(\alpha_{11}+\alpha_5)\big)\big],\\
&m_{33}=-I_0[\alpha_1-\mu(\alpha_9+\alpha_3)]\\
&+I_2[(\alpha_9+\alpha_3)-\mu(\alpha_{13}+\alpha_5+2\alpha_{11})],\\
&m_{34}=-I_0[\alpha_1-\mu(\alpha_9+\alpha_3)]\\
&+J_2[(\alpha_9+\alpha_3)-\mu(\alpha_{13}+\alpha_5+2\alpha_{11})],\\
&m_{41}=-J_1[\alpha_9-\mu(\alpha_{13}+\alpha_{11})],\\
&m_{42}=-J_1[\alpha_3-\mu(\alpha_{11}+\alpha_5)],\\
&m_{43}=-I_0[\alpha_1-\mu(\alpha_9+\alpha_3)]\\
&+J_2[(\alpha_9+\alpha_3)-\mu(\alpha_{13}+\alpha_5+2\alpha_{11})],\\
&m_{44}=-I_0[\alpha_1-\mu(\alpha_9+\alpha_3)]\\
&+K_2[(\alpha_9+\alpha_3)-\mu(\alpha_{13}+\alpha_5+2\alpha_{11})]
\end{aligned}
\tag{28b}
$$

With

$$
\begin{aligned}
(\alpha_1,\alpha_3,\alpha_5)&=\int_0^b\int_0^a (X_mY_n, X_mY_n'', X_mY_n'''')\,X_mY_n dxdy\\
(\alpha_2,\alpha_4,\alpha_{10})&=\int_0^b\int_0^a (X_mY_n', X_mY_n'', X_m''Y_n')\,X_mY_n' dxdy\\
(\alpha_6,\alpha_8,\alpha_{12})&=\int_0^b\int_0^a (X_m'Y_n, X_m'Y_n'', X_m'''Y_n)\,X_m'Y_n dxdy\\
(\alpha_7,\alpha_9,\alpha_{11},\alpha_{13})&\\
=\int_0^b\int_0^a &(X_m'Y_n', X_m''Y_n, X_m'Y_n'', X_m''''Y_n)\,X_mY_n dxdy
\end{aligned}
\tag{29}
$$

The nontrivial solution of the present problem is found equating the determinant of equation (27) to zero.

4. The numerical results and discussion

Since there is no study regarding free vibration analyses of FG-GNPR nanoplates in the open literature, to validate the accuracy of the present method, the results are first

Table 4 The first non-dimensional natural frequency $\overline{\omega} = \omega h\sqrt{\rho_m/E_m}$ of the SSSS FG-GNPR square nanoplate

a/h	Pattern	Theories	μ					
			0	1	2	3	4	5
5	Pure epoxy	(Phung-Van *et al*. 2021)	0.2132	0.1948	0.1805	0.1690	0.1594	0.1513
		Present	0.2132	0.1948	0.1805	0.1689	0.1594	0.1513
	UD	(Phung-Van *et al*. 2021)	0.2285	0.2088	0.1935	0.1811	0.1708	0.1621
		Present	0.2285	0.20883	0.19349	0.18110	0.17082	0.16211
	FG-O	(Phung-Van *et al*. 2021)	0.2241	0.2048	0.1898	0.1776	0.1675	0.1590
		Present	0.22417	0.20486	0.18981	0.17766	0.16757	0.15903
	FG-X	(Phung-Van *et al*. 2021)	0.2326	0.2126	0.1969	0.1843	0.1739	0.1650
		Present	0.23257	0.21254	0.19692	0.18431	0.17385	0.16499
	FG-A	(Phung-Van *et al*. 2021)	0.2281	0.2085	0.1931	0.1808	0.1705	0.1618
		Present	0.22812	0.20847	0.19316	0.18079	0.17052	0.16183
10	Pure epoxy	(Phung-Van *et al*. 2021)	0.0584	0.0534	0.0495	0.0463	0.0437	0.0415
		Present	0.0584	0.0534	0.0495	0.0463	0.0437	0.0415
	UD	(Phung-Van *et al*. 2021)	0.0626	0.0572	0.0530	0.0496	0.0468	0.0444
		Present	0.06261	0.05721	0.0530	0.04962	0.04680	0.04441
	FG-O	(Phung-Van *et al*. 2021)	0.0611	0.0559	0.0518	0.0484	0.0457	0.0434
		Present	0.06112	0.55857	0.05175	0.04843	0.04569	0.04336
	FG-X	(Phung-Van *et al*. 2021)	0.0641	0.0585	0.0542	0.0508	0.0479	0.0454
		Present	0.06406	0.05854	0.05424	0.05076	0.04788	0.04544
	FG-A	(Phung-Van *et al*. 2021)	0.0625	0.0571	0.0529	0.0495	0.0467	0.0443
		Present	0.06249	0.05711	0.05291	0.04952	0.04671	0.04433
20	Pure epoxy	(Phung-Van *et al*. 2021)	0.0150	0.0137	0.0127	0.0119	0.0112	0.0106
		Present	0.0150	0.0137	0.0127	0.0119	0.0112	0.0106
	UD	(Phung-Van *et al*. 2021)	0.0161	0.0147	0.0136	0.0127	0.0120	0.0114
		Present	0.01607	0.01469	0.01361	0.01274	0.01201	0.0114
	FG-O	(Phung-Van *et al*. 2021)	0.0157	0.0143	0.0133	0.0124	0.0117	0.0111
		Present	0.01567	0.01432	0.01326	0.01241	0.01171	0.01111
	FG-X	(Phung-Van *et al*. 2021)	0.0165	0.0151	0.0140	0.0131	0.0123	0.0117
		Present	0.01647	0.01505	0.01395	0.01306	0.01231	0.01169
	FG-A	(Phung-Van *et al*. 2021)	0.0160	0.0147	0.0136	0.0127	0.0120	0.0114
		Present	0.01604	0.01466	0.01358	0.01271	0.01199	0.01138
50	Pure epoxy	(Phung-Van *et al*. 2021)	0.0024	0.0022	0.0020	0.0019	0.0018	0.0017
		Present	0.0024	0.0022	0.0020	0.0019	0.0018	0.0017
	UD	(Phung-Van *et al*. 2021)	0.0026	0.0024	0.0022	0.0021	0.0019	0.0018
		Present	0.00259	0.00236	0.00219	0.00205	0.00193	0.00183
	FG-O	(Phung-Van *et al*. 2021)	0.0025	0.0023	0.0021	0.0020	0.0019	0.0018
		Present	0.00252	0.00230	0.00213	0.00200	0.00188	0.00179
	FG-X	(Phung-Van *et al*. 2021)	0.0027	0.0024	0.0023	0.0021	0.0020	0.0019
		Present	0.00265	0.00242	0.00225	0.00210	0.00198	0.00188
	FG-A	(Phung-Van *et al*. 2021)	0.0026	0.0024	0.0022	0.0021	0.0019	0.0018
		Present	0.00258	0.00236	0.00219	0.00205	0.00193	0.00183

compared with two examples that include FG-GNPR nanoplate and isotropic nanoplates are performed in Section 4.1. Then, the analysis is extended to FG-GNPR nanoplate with following material properties: E_m=3.0GPa, ν_m=0.34, ρ_m=1200 kg/m^3.

4.1 Verification

4.1.1 FG-GRC plates

Consider a simply supported square plate with the length a = 0.45, the weight fraction of GNPs gGNP = 1%,

Table 5 The first non-dimensional natural frequency $\overline{\omega} = \omega h\sqrt{\rho_m/E_m}$ of the CCCC FG-GNPR square nanoplate

a/h	Pattern	Theories	μ					
			0	1	2	3	4	5
5	Pure epoxy	(Phung-Van *et al*. 2021)	0.3316	0.2988	0.2739	0.2542	0.2382	0.2248
		Present	0.3518	0.3119	0.2831	0.2611	0.2435	0.2290
	UD	(Phung-Van *et al*. 2021)	0.3555	0.3203	0.2936	0.2725	0.2553	0.2409
		Present	0.37716	0.33441	0.30352	0.27986	0.26099	0.24549
	FG-O	(Phung-Van *et al*. 2021)	0.3519	0.3168	0.2903	0.2694	0.2523	0.2381
		Present	0.37280	0.33047	0.29990	0.27650	0.25783	0.24250
	FG-X	(Phung-Van *et al*. 2021)	0.3586	0.3232	0.2964	0.2752	0.2578	0.2434
		Present	0.38085	0.33776	0.30661	0.28274	0.26370	0.24805
	FG-A	(Phung-Van *et al*. 2021)	0.3551	0.3199	0.2932	0.2721	0.2549	0.2406
		Present	0.37667	0.33396	0.30311	0.27948	0.26064	0.24515
10	Pure epoxy	(Phung-Van *et al*. 2021)	0.1008	0.0906	0.0829	0.0769	0.072	0.0679
		Present	0.1052	0.0935	0.0849	0.0784	0.0731	0.0688
	UD	(Phung-Van *et al*. 2021)	0.1081	0.0971	0.0889	0.0824	0.0771	0.0727
		Present	0.11280	0.10020	0.09105	0.08402	0.07841	0.07378
	FG-O	(Phung-Van *et al*. 2021)	0.1059	0.0951	0.0871	0.0807	0.0755	0.0712
		Present	0.11047	0.09812	0.08916	0.08228	0.07677	0.07225
	FG-X	(Phung-Van *et al*. 2021)	0.1101	0.0990	0.0906	0.0840	0.0786	0.0742
		Present	0.11502	0.10217	0.09285	0.08568	0.07996	0.07524
	FG-A	(Phung-Van *et al*. 2021)	0.1079	0.0969	0.0887	0.0822	0.0770	0.0726
		Present	0.11261	0.10002	0.09089	0.08387	0.07827	0.07365
20	Pure epoxy	(Phung-Van *et al*. 2021)	0.0269	0.0242	0.0221	0.0205	0.0192	0.0181
		Present	0.0279	0.0248	0.0225	0.0208	0.0194	0.0183
	UD	(Phung-Van *et al*. 2021)	0.0289	0.0259	0.0237	0.0220	0.0206	0.0194
		Present	0.02993	0.02662	0.02421	0.02235	0.02086	0.01964
	FG-O	(Phung-Van *et al*. 2021)	0.0282	0.0253	0.0231	0.0214	0.0201	0.0189
		Present	0.02920	0.02597	0.02361	0.02180	0.02035	0.01916
	FG-X	(Phung-Van *et al*. 2021)	0.0296	0.0265	0.0243	0.0225	0.0211	0.0199
		Present	0.03065	0.02725	0.02478	0.02288	0.02136	0.02011
	FG-A	(Phung-Van *et al*. 2021)	0.0288	0.0259	0.0237	0.0219	0.0205	0.0194
		Present	0.02988	0.02657	0.02416	0.02231	0.02082	0.01960
50	Pure epoxy	(Phung-Van *et al*. 2021)	0.0044	0.0040	0.0036	0.0033	0.0031	0.0030
		Present	0.0045	0.0040	0.0036	0.0034	0.0031	0.0029
	UD	(Phung-Van *et al*. 2021)	0.0047	0.0042	0.0039	0.0036	0.0034	0.0032
		Present	0.00487	0.00434	0.00394	0.00364	0.00340	0.0032
	FG-O	(Phung-Van *et al*. 2021)	0.0046	0.0041	0.0038	0.0035	0.0033	0.0031
		Present	0.00475	0.00422	0.00384	0.00355	0.00331	0.00312
	FG-X	(Phung-Van *et al*. 2021)	0.0048	0.0043	0.0040	0.0037	0.0034	0.0032
		Present	0.00500	0.00445	0.00404	0.00373	0.00349	0.00328
	FG-A	(Phung-Van *et al*. 2021)	0.0047	0.0042	0.0039	0.0036	0.0034	0.0032
		Present	0.00486	0.00433	0.00394	0.00363	0.00339	0.00319

length-to-thickness ratio a/h=10, and NL= 10. The material properties of GNPs are defined as: EGNP = 1.01TPa, GNP = 0.186, ρGNP = 1060 kg⁄m^3, lGNP = 2.5 μm, wGNP = 1.5 μm, hGNP = 1.5 nm.

The first two natural frequencies of the FG GNPRC plates are summarized in Table 2. It can be observed that the present results are in good agreement with those of the reference solutions for all patterns and pure epoxy.

Table 6 The first non-dimensional natural frequency $\overline{\omega} = \omega h\sqrt{\rho_m/E_m}$ of the CSCS FG-GNPR square nanoplate

a/h	Pattern	μ					
		0	1	2	3	4	5
5	Pure epoxy	0.29567	0.26598	0.24374	0.22629	0.21212	0.20031
	UD	0.31692	0.28509	0.26126	0.24255	0.22736	0.21470
	FG-O	0.31236	0.28096	0.25745	0.23900	0.22403	0.21155
	FG-X	0.32096	0.28877	0.26465	0.24571	0.23033	0.21752
	FG-A	0.31646	0.28467	0.26087	0.24219	0.22702	0.21438
10	Pure epoxy	0.08541	0.07693	0.07056	0.06555	0.06147	0.05807
	UD	0.09152	0.08244	0.07561	0.07024	0.06587	0.06223
	FG-O	0.08951	0.08062	0.07394	0.06869	0.06442	0.06086
	FG-X	0.09345	0.08418	0.07721	0.07172	0.06727	0.06355
	FG-A	0.09136	0.08229	0.07547	0.07011	0.06575	0.06212
20	Pure epoxy	0.02235	0.02014	0.01849	0.01718	0.01611	0.01523
	UD	0.02394	0.02158	0.01980	0.01840	0.01726	0.01631
	FG-O	0.02335	0.02104	0.01931	0.01794	0.01683	0.01590
	FG-X	0.02453	0.02211	0.02028	0.01885	0.01768	0.01671
	FG-A	0.02390	0.02154	0.01976	0.01837	0.01723	0.01628
50	Pure epoxy	0.00363	0.00327	0.00299	0.00279	0.00262	0.00247
	UD	0.00388	0.00350	0.00321	0.00298	0.00280	0.00264
	FG-O	0.00378	0.00341	0.00313	0.00291	0.00273	0.00257
	FG-X	0.00398	0.00359	0.00329	0.00306	0.00287	0.00271
	FG-A	0.00387	0.00349	0.00320	0.00298	0.00279	0.00264

4.1.2 Isotropic nanoplate

Table 3 presents the comparison of sinusoidal shear deformation theory SSDT and FSDT with the present method. The analysis was performed assuming a simply supported square isotropic nanoplates (length a = 10, thickness h). The material properties can be given as E=3×106, ν = 0.3, ρ = 1.

4.2 Free vibration analysis

4.2.1 Square nanoplate

At first, the FG-GNPRC square plate with the length a=10, GNPs weight fraction g_{GNP}= 1%, and ten layers N_L= 10 is considered. Here, the material properties of GNPs are given as: E_{GNP}= 1.01 TPa, ν_{GNP}= 0.186, ρ_{GNP}= 1062.5 kg⁄m^3, l_{GNP}= 2.5 nm, w_{GNP}= 1.5 nm, h_{GNP}= 0.3 nm.

Tables 3, 4, 5, and 6, respectively, list the first non-dimensional natural frequency of simply supported (SSSS), CCCC, CSCS, and FCFC FG-GNPR nanoplate with different values of length-to-thickness ratio and nonlocal parameter.

Table 2 provides a comprehensive comparison of results from four different studies: (Sobhy, 2013), (Reddy *et al*. 2018), (Phung-Van *et al*. 2021), and the present study. The analysis is performed on different material patterns: Pure epoxy, UD, FG-O, FG-X, and FG-A, across two modes. In Mode 1, the values for Pure epoxy are nearly identical across all studies, with a minimal difference of 0.68% between the present study and the reference. In Mode 1, the UD pattern values are generally higher than those for pure epoxy and FG-O, but lower than FG-X, with FG-A falling in between UD and FG-O. In Mode 2, a similar trend is observed with UD values higher than FG-O but lower than FG-X, and FG-A values again being intermediate. Across both modes, FG-X consistently exhibits the highest natural frequency, followed by UD, FG-A, and FG-O, highlighting the varying performance characteristics of these material patterns.

Table 3 presents the values of the first non-dimensional natural frequency of FG-GNPR square nanoplates with SSSS boundary conditions versus *a/h*, different theories: SSDT, FSDT, RPT, and the present study, for the values of the parameter, μ, ranging from 0 to 5). An increase in the parameter decreases the natural frequency of an isotropic square nanoplate.

Table 4 compares the values of the first non-dimensional natural frequency of FG-GNPR square nanoplates with SSSS boundary conditions versus *a/h*, different material patterns (Pure epoxy, UD, FG-O, FG-X, FG-A) and theories with different parameter values (0 to 5). Generally, the parameter *a/h* values increase significantly, indicating a reduction in the stiffness of the structure, which thereby reduces the natural frequency because the smaller FG-GNPR nanoplate is stiffer than the larger one. Upon estimating the percentage change in the natural frequency, it is found that for *a/h* = 5 to *a/h* = 10, the change is around 72 %, for *a/h* = 10 to a/h = 20, it is 74 %, while for *a/h* = 20 to *a/h* = 50, it is 84 % which indicates that the reduction in stiffness significantly higher for larger *a/h* ratios. Similarly, incrementing the parameter μ, from 1 to 5, decreases the

Table 7 The first non-dimensional natural frequency $\overline{\omega} = \omega h\sqrt{\rho_m/E_m}$ of the FCFC FG-GNPR square nanoplate

a/h	Pattern	μ					
		0	1	2	3	4	5
5	Pure epoxy	0.36259	0.32302	0.29409	0.27176	0.25385	0.23906
	UD	0.38870	0.34628	0.31527	0.29132	0.27212	0.25627
	FG-O	0.38493	0.34281	0.31204	0.28830	0.26927	0.25356
	FG-X	0.39176	0.34911	0.31791	0.29381	0.27447	0.25851
	FG-A	0.38823	0.34585	0.31487	0.29095	0.27177	0.25594
10	Pure epoxy	0.11080	0.09891	0.09017	0.08340	0.07795	0.07346
	UD	0.11874	0.10599	0.09663	0.08937	0.08354	0.07872
	FG-O	0.11639	0.10388	0.09470	0.08759	0.08187	0.07715
	FG-X	0.12095	0.10798	0.09844	0.09105	0.08511	0.08020
	FG-A	0.11854	0.10581	0.09646	0.08922	0.08340	0.07858
20	Pure epoxy	0.02967	0.02653	0.02421	0.02241	0.02096	0.01976
	UD	0.03179	0.02842	0.02594	0.02401	0.02245	0.02116
	FG-O	0.03102	0.02773	0.02531	0.02342	0.02191	0.02065
	FG-X	0.03254	0.02909	0.02655	0.02457	0.02298	0.02166
	FG-A	0.03173	0.02837	0.02589	0.02396	0.02241	0.02112
50	Pure epoxy	0.00485	0.00434	0.00396	0.00367	0.00343	0.00323
	UD	0.00519	0.00464	0.00424	0.00392	0.00367	0.00346
	FG-O	0.05064	0.00452	0.00413	0.00382	0.00358	0.00337
	FG-X	0.00532	0.00476	0.00435	0.00402	0.00376	0.00355
	FG-A	0.00518	0.00464	0.00423	0.00392	0.00366	0.00345

frequency by 8.6 %, 7.3 %, 6.3 %, 5.6%, and 5 %, which indicates that the difference in magnitude becomes insignificant over a specific value of parameter μ.

Table 5 compares the values of the first non-dimensional natural frequency of FG-GNPR nanoplates with CCCC boundary conditions versus *a/h* different material patterns and theories with different parameter values. Upon estimating the percentage change in the natural frequency, it is found that for *a/h* = 5 to *a/h* = 10, the change is around 70 %, for *a/h* = 10 to *a/h* = 20, it is 73.2 %, while for *a/h* = 20 to *a/h* = 50, it is 83 % which indicates that the reduction in stiffness significantly higher for larger *a/h* ratios. Similarly, incrementing the parameter from 1 to 5 decreases the frequency by 9.8%, 8.3%, 7.2%, 6.3%, and 5.6 %, which means beyond a particular value of parameter μ, the difference in the magnitude becomes negligible.

Table 6 presents the values of the first non-dimensional natural frequency of FG-GNPR nanoplates with CSCS boundary conditions versus *a/h* different material patterns. Upon estimating the percentage change in the natural frequency, it was found that for *a/h* = 5 to *a/h* = 10, the change is around 71 %, for *a/h* = 10 to *a/h* = 20, it is 73.82 %, while for *a/h* = 20 to *a/h*= 50, it is 83.7 % which indicates that the reduction in stiffness significantly higher for larger a/h ratios. Similarly, incrementing the parameter from 1 to 5 decreases the frequency by 9.9 %, 8.3 %, 7.1 %, 6.2%, and 5.5 %, which shows beyond a particular value of parameter μ, the difference in the magnitude becomes negligible.

Table 7 shows the values of the first non-dimensional

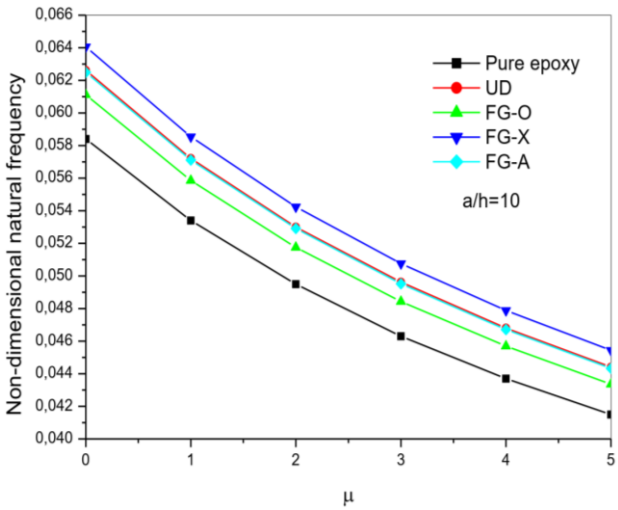

Fig. 2 The variation of the first non-dimensional natural frequency $\overline{\boldsymbol{\omega}}$ vs nonlocal parameter $\boldsymbol{\mu}$ of the SSSS FG GNPRC square nanoplate

natural frequency of FG-GNPR nanoplates with FCFC boundary conditions versus *a/h* different material patterns. Upon estimating the percentage change in the natural frequency, it was found that for *a/h* = 5 to *a/h* = 10, the change is around 69 %, for *a/h* = 10 to *a/h* = 20, it is 73 %, while for *a/h* = 20 to a/h = 50, it is 83.6 % which indicates that the reduction in stiffness significantly higher for larger a/h ratios. Similarly, incrementing the parameter from 1 to 5 decreases the frequency by 9.8 %, 8.9 %, 7.6 %, 6.6%, and 5.7 %.

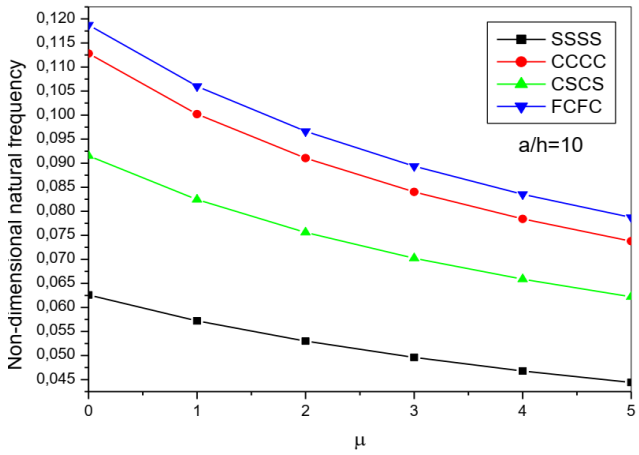

Fig. 3 The variation of the first non-dimensional natural frequency $\overline{\omega}$ for UD- pattern vs nonlocal parameter μ under various boundary conditions

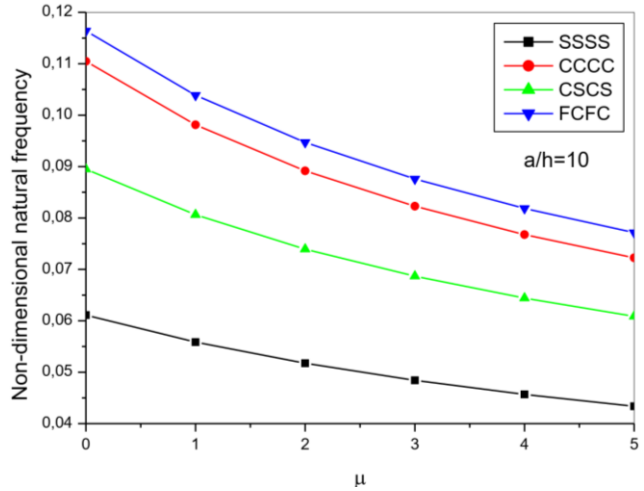

Fig. 4 The variation of the first non-dimensional natural frequency $\overline{\omega}$ for FG-O pattern vs nonlocal parameter μ under various boundary conditions

Fig. 2 shows the variation of non-dimensional frequency for varying nonlocal parameters for SSSS boundary conditions. It can be seen that pure epoxy yields the lowest frequency and FG-X type the maximum. The other gradings show intermediate results, in which FG-A and UD give similar frequency values, and their magnitude is higher than that of the FG-O type.

Fig. 3 demonstrates the natural frequency for different boundary conditions for the UD pattern, out of all conditions, FCFC yields the maximum frequency, followed by CCCC, CSCS, and SSSS.

Similarly, Figs. 4-6 demonstrates the natural frequency values for FG-O, FG-X and FG-A. From the analysis, it is found that for all cases like UD, the natural frequency follows a similar trend. Also, in all the cases, the difference in the frequency value is very high when FCFC and SSSS are compared, while it is much less for FCFC and CCCC. It is interesting to note that the frequency values of CSCS remains in the middle of the results of SSSS and FCFC boundary conditions.

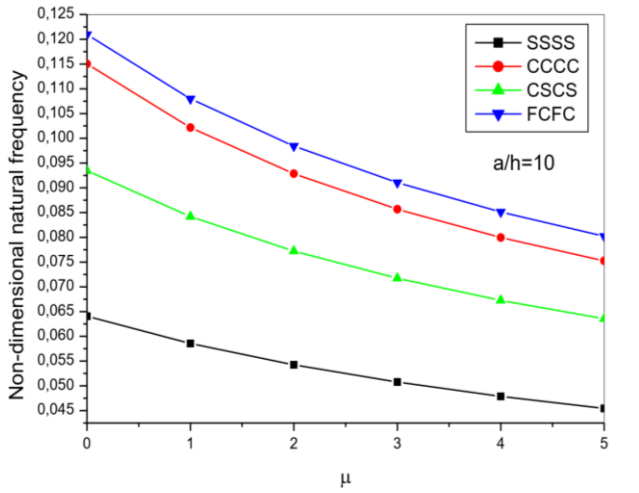

Fig. 5 The variation of the first non-dimensional natural frequency $\overline{\omega}$ for FG-X pattern vs nonlocal parameter μ under various boundary conditions

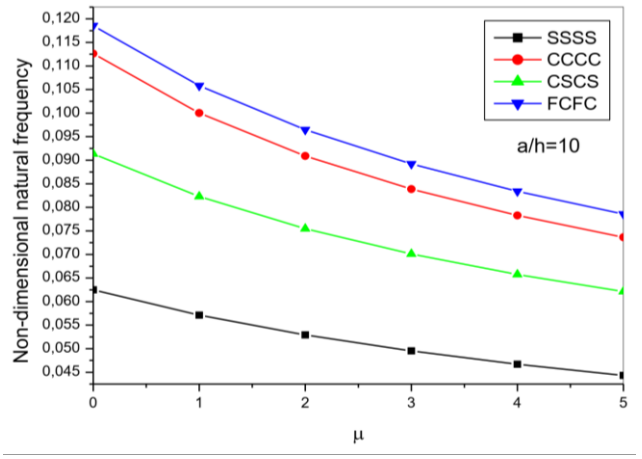

Fig. 6 The variation of the first non-dimensional natural frequency $\overline{\omega}$ for FG-A pattern vs nonlocal parameter μ under various boundary conditions

5. Conclusions

The study demonstrates valuable insights into the natural frequency behaviour of pure epoxy, UD, FG-O, FG-X, and FG-A, FG-GNPR nanoplates under various boundary conditions. It highlights the importance of considering factors such as aspect ratios, boundary conditions, and nonlocal parameters in the structural analysis and design of FG-GNPR nanoplates.

Briefly, the following noteworthy conclusions have been identified:

1. Each type of boundary condition yields different natural frequency values. For instance, the natural frequency obtained is maximum for FCFC followed by CCCC, and CSCS and yields the least value for SSSS.

2. The variation in the magnitude of natural frequency for varying parameters *a/h* and μ is the same for CCCC, CSCS, and FCFC, whereas there is a slight variation for SSSS. Also, the change for the SSSS boundary condition is comparatively lower.

3. For a fixed aspect ratio (*a/h*=5), varying the *a/h* ratio also affects the frequencies. Generally, higher *a/h* ratios lead to lower frequencies across different boundary conditions and parameter μ.

4. As the parameter (*m*) increases, the frequencies generally decrease. This trend is observed across different boundary conditions and *a/h* ratios.

5. The natural frequency results for FG-GNPR nanoplates for different boundary conditions and geometry parameters indicate that lower geometry parameters generally result in higher natural frequency, indicating enhanced structural stability.

The study provides valuable insights for design engineers on how different parameters and boundary conditions influence the natural frequency of FG-GNPR nanoplates.

References

Abdalla, H.M.A., Casagrande, D., De Bona, F., De Monte, T., Sortino, M. and Totis, G. (2021), "An optimized pressure vessel obtained by metal additive manufacturing: Preliminary results", *Int. J. Press. Vess. Pip.*, **192**, 104434. https://doi.org/10.1016/j.ijpvp.2021.104434.

Abedini Baghbadorani, A. and Kiani, Y. (2021), "Free vibration analysis of functionally graded cylindrical shells reinforced with graphene platelets", *Compos. Struct.*, **276**, 114546. https://doi.org/10.1016/j.compstruct.2021.114546.

Affdl, J.C.H. and Kardos, J.L. (1976), "The Halpin-Tsai equations: A review", *Polym. Eng. Sci.*, **16**(5), 344-352. https://doi.org/10.1002/pen.760160512.

Aghababaei, R. and Reddy, J.N. (2009), "Nonlocal third-order shear deformation plate theory with application to bending and vibration of plates", *J. Sound Vib.*, **326**(1), 277-289. https://doi.org/10.1016/j.jsv.2009.04.044.

Abdalla, H.M.A., Casagrande, D., De Bona, F., De Monte, T., Sortino, M. and Totis, G. (2021), "An optimized pressure vessel obtained by metal additive manufacturing: Preliminary results", *Int. J. Press. Vess. Pip.*, **192**, 104434. https://doi.org/10.1016/j.ijpvp.2021.104434.

Abedini Baghbadorani, A. and Kiani, Y. (2021), "Free vibration analysis of functionally graded cylindrical shells reinforced with graphene platelets", *Compos. Struct.*, **276**, 114546. https://doi.org/10.1016/j.compstruct.2021.114546.

Affdl, J.C.H. and Kardos, J.L. (1976), "The Halpin-Tsai equations: A review", *Polym. Eng. Sci.*, **16**(5), 344-352. https://doi.org/10.1002/pen.760160512.

Aghababaei, R. and Reddy, J.N. (2009), "Nonlocal third-order shear deformation plate theory with application to bending and vibration of plates", *J. Sound Vib.*, **326**(1), 277-289. https://doi.org/10.1016/j.jsv.2009.04.044.

Ait Atmane, H., Tounsi, A., Mechab, I., Adda Bedia, E.A. (2010), "Free vibration analysis of functionally graded plates resting on Winkler-Pasternak elastic foundations using a new shear deformation theory", *Int. J. Mech. Mater. Des.*, **6**(113-121). https://doi.org/10.1007/s10999-010-9110-x.

Ait Atmane, H., Tounsi, A. and Bernard, F. (2017), "Effect of thickness stretching and porosity on mechanical response of a functionally graded beams resting on elastic foundations", *Int. J. Mech. Mater. Des.*, **13**(71-84). https://doi.org/10.1007/s10999-015-9318-x.

Ait Atmane, R., Mahmoudi, N., Bennai, R., Ait Atmane, H. and Tounsi, A. (2021). Investigation on the dynamic response of porous FGM beams resting on variable foundation using a new higher order shear deformation theory", *Steel Compos. Struct.*, **39**(1), 95-107. https://doi.org/10.12989/SCS.2021.39.1.095.

Akinwamide, S.O., Abe, B.T., Akinribide, O.J., Obadele, B.A. and Olubambi, P.A. (2020), "Characterization of microstructure, mechanical properties and corrosion response of aluminium-based composites fabricated via casting—a review", *Int. J. Adv. Manuf. Technol.*, **109**(3-4), 975-991. https://doi.org/10.1007/s00170-020-05703-1.

Al-Shafaie, S.H., Radhi, N.S. and Hussein, M.A. (2021), "Preparation and investigation of microstructure and wear properties of functionally graded materials of Aluminum-Nickel alloys", *J. Phys.*, **1973**(1), 012099. https://doi.org/10.1088/1742-6596/1973/1/012099

Arefi, M., Mohammad-Rezaei Bidgoli, E., Dimitri, R. and Tornabene, F. (2018), "Free vibrations of functionally graded polymer composite nanoplates reinforced with graphene nanoplatelets", *Aerosp. Sci. Technol.*, **81**, 108-117. https://doi.org/10.1016/j.ast.2018.07.036.

Arefi, M. and Zenkour, A.M. (2016), "Employing sinusoidal shear deformation plate theory for transient analysis of three layers sandwich nanoplate integrated with piezo-magnetic face-sheets", *Smart Mater. Struct.*, **25**(11), 115040. https://doi.org/10.1088/0964-1726/25/11/115040.

Aruri, D., Adepu, K., Adepu, K. and Bazavada, K. (2013), "Wear and mechanical properties of 6061-T6 aluminum alloy surface hybrid composites [(SiC+Gr) and (SiC+Al_2O_3)] fabricated by friction stir processing", *J. Mater. Res. Technol.*, **2**(4), 362-369. https://doi.org/10.1016/j.jmrt.2013.10.004.

Zare, E., Voronkova, D.K., Faraji, O., Aghajanirefah, H., Nia, H. M., Gholami, M. and Azandariani, M.G. (2024), "Assessment of nonlocal nonlinear free vibration of bi-directional functionally-graded Timoshenko nanobeams", *Adv. Nano Res.*, **16**(5), 473-487. https://doi.org/10.12989/anr.2024.16.5.473

Avcar, M. (2019), "Free vibration of imperfect sigmoid and power law functionally graded beams", *Steel Compos. Struct.*, **30**(6), 603-615. https://doi.org/10.12989/SCS.2019.30.6.603.

Avcar, M., Hadji, L. and Akan, R. (2022), "The influence of Winkler-Pasternak elastic foundations on the natural frequencies of imperfect functionally graded sandwich beams", *Geomech. Eng.*, **31**(1), 99-112. https://doi.org/10.12989/gae.2022.31.1.099.

Benoit, M.J., Mazur, M., Easton, M.A. and Brandt, M. (2021), "Effect of alloy composition and laser powder bed fusion parameters on the defect formation and mechanical properties of Inconel 625", *Int. J. Adv. Manuf. Technol.*, **114**(3-4), 915-927. https://doi.org/10.1007/s00170-021-06957-z.

Bisht, A., Srivastava, M., Kumar, R.M., Lahiri, I. and Lahiri, D. (2017), "Strengthening mechanism in graphene nanoplatelets reinforced aluminum composite fabricated through spark plasma sintering", *Mater. Sci. Eng. A*, **695**, 20-28. https://doi.org/10.1016/j.msea.2017.04.009.

Bykov, Y.V., Egorov, S.V., Eremeev, A.G., Plotnikov, I.V., Rybakov, K.I., Semenov, V.E., Sorokin, A.A. and Holoptsev, V.V. (2012), "'Fabrication of metal-ceramic functionally graded materials by microwave sintering'", *Inorgan. Mater. Appl. Res.*, **3**(3), 61-269. https://doi.org/10.1134/S2075113312030057.

Chen, W., Wang, Q., Zai, C., Ma, C., Zhu, Y. and He, W. (2001), "Functionally graded Zn-Al-Si in-situ composites fabricated by centrifugal casting", *J. Mater. Sci. Lett.*, **20(**9), 823-826. https://doi.org/10.1023/A:1010954527987.

Cong, P.H. and Duc, N.D. (2023), "Effect of nonlocal parameters and Kerr foundation on nonlinear static and dynamic stability of micro/nano plate with graphene platelet reinforcement", *Thin Wall. Struct.*, **182**, 110146. https://doi.org/10.1016/j.tws.2022.110146.

Cornacchia, F., Fabbrocino, F., Fantuzzi, N., Luciano, R. and Penna, R. (2019), "Analytical solution of cross- and angle-ply

nano plates with strain gradient theory for linear vibrations and buckling", *Mech. Adv. Mater. Struct.*, **28**(12), 1201-1215. https://doi.org/10.1080/15376494.2019.1655613.

Cottrell, J.A., Reali, A., Bazilevs, Y. and Hughes, T.J.R. (2006), "Isogeometric analysis of structural vibrations", *Comput. Meth. Appl. Mech. Eng.*, **195**(41-43), 5257-5296. https://doi.org/10.1016/j.cma.2005.09.027.

Dahmane, M., Benadouda, M., Fellah, A., Saimi, A., Ait Atmane, H.,and Bensaid, I. (2023), "Porosities-dependent wave propagation in bi-directional functionally graded cantilever beam with higher-order shear model", *Mech. Adv. Mater. Struct.*, **30**, 1-11. https://doi.org/10.1080/15376494.2023.2253546.

Debbaghi, S., Dahmane, M., Benadouda, M., Ait Atmane, H., Bendenia, N. and Hadji, L. (2024), "Wave propagation of bi-directional porous FG beams using Touratier's higher-order shear deformation beam theory", *Coupled Syst. Mech.*, **13**(1), 43-60. https://doi.org/10.12989/csm.2024.13.1.043.

Djilali Djebbour, K., Nebab, M., Ait Atmane, H., Alghanmi, R., Hadji, L. and, Bennai, R. (2024), "An enhanced quasi-3D HSDT for free vibration analysis of porous FG-CNT beams on a new concept of orthotropic VE-foundations", *Mech. Adv. Mater. Struct.*, 1-17. https://doi.org/10.1080/15376494.2024.2356728.

Ebrahimi, F. and Jafari, A. (2017), "Investigating vibration behavior of smart imperfect functionally graded beam subjected to magnetic-electric fields based on refined shear deformation theory", *Adv. Nano Res.*, **5**(4), 281-301. https://doi.org/10.12989/anr.2017.5.4.281.

Gao, K., Gao, W., Chen, D. and Yang, J. (2018), "Nonlinear free vibration of functionally graded graphene platelets reinforced porous nano-composite plates resting on elastic foundation", *Compos. Struct.*, **204**, 831-846. https://doi.org/10.1016/j.compstruct.2018.08.013.

Hadji, L. and Avcar, M. (2021), "Nonlocal free vibration analysis of porous FG nanobeams using hyperbolic shear deformation beam theory", *Adv. Nano Res.*, **10**(3), 281-293. https://doi.org/10.12989/ANR.2021.10.3.281.

Hadji, L., Bernard, F. and Zouatnia, N. (2023), "Bending and Free vibration analysis of Porous-Functionally-Graded (PFG) beams resting on elastic foundations", *Fluid Dyn. Mater. Proc.*, **19**(4), https://doi.org/10.32604/fdmp.2022.022327.

Hadji, L., Plevris, V., Madan, R. and Ait Atmane, H., (2024a), "Multi-directional functionally graded sandwich plates: Buckling and free vibration analysis with refined plate models under various boundary conditions", *Computation*, **12**(4). https://doi.org/10.3390/computation12040065.

Hadji, L., Madan, R., Atmane, H. A., Bernard, F., Zouatnia, N. and Safa, A. (2024b), "Thermal buckling Analysis of functionally graded plates using trigonometric shear deformation theory for temperature-dependent material properties", *Struct. Eng. Mech.*, **91**(6), 539-549. https://doi.org/10.12989/sem.2024.91.6.539.

Huang, S.J., Kannaiyan, S. and Subramani, M. (2022), "Effect of nano-Nb_2O_5 on the microstructure and mechanical properties of AZ31 alloy matrix nanocomposites", *Adv. Nano Res.*, **13**(4), 407-416. https://doi.org/10.12989/ANR.2022.13.4.407.

Hughes, T.J.R., Cottrell, J.A. and Bazilevs, Y. (2005), "Isogeometric analysis: CAD, finite elements, NURBS, exact geometry and mesh refinement", *Comput. Meth. Appl. Mech. Eng.*, **194**(39-41), 4135-4195. https://doi.org/10.1016/j.cma.2004.10.008.

Jalali, S.K. and Heshmati, M. (2020), "Vibration analysis of tapered circular poroelastic plates with radially graded porosity using pseudo-spectral method", *Mech. Mater.*, **140**, 103240. https://doi.org/10.1016/j.mechmat.2019.103240.

Kitipornchai, S., Chen, D. and Yang, J. (2017), "Free vibration and elastic buckling of functionally graded porous beams reinforced by graphene platelets", *Mater. Des.*, **116**, 656-665. https://doi.org/10.1016/j.matdes.2016.12.061.

Kolman, R., Sorokin, S., Bastl, B., Kopačka, J. and Plešek, J. (2015), "Isogeometric analysis of free vibration of simple shaped elastic samples", *J. Acoust. Soc. Am.*, **137**(4), 2089-2100. https://doi.org/10.1121/1.4916199.

Lal, R. and Saini, R. (2020), "Vibration analysis of functionally graded circular plates of variable thickness under thermal environment by generalized differential quadrature method", *J. Vib. Control*, **26**(1-2), 73-87. https://doi.org/10.1177/1077546319876389.

Li, X., Wang, T., Liu, F. and Zhu, Z. (2021), "Computer simulation of the nonlinear static behavior of axially functionally graded microtube with porosity", *Adv. Nano Res.*, **11**(4), 437-451. https://doi.org/10.12989/anr.2021.11.4.437.

Li, L. and Zhang, D.G. (2016), "Free vibration analysis of rotating functionally graded rectangular plates", *Compos. Struct.*, **136**, 493-504. https://doi.org/10.1016/j.compstruct.2015.10.013.

Lieu, Q.X., Lee, D., Kang, J. and Lee, J. (2019), "NURBS-based modeling and analysis for free vibration and buckling problems of in-plane bi-directional functionally graded plates", *Mech. Adv. Mater. Struct.*, **26**(12), 1064-1080. https://doi.org/10.1080/15376494.2018.1430273.

Liu, C.-F. and Lee, Y.-T. (2000), "finite element analysis of three-dimensional vibrations of thick circular and annular plates", *J. Sound Vib.*, **233**(1), 63-80. https://doi.org/10.1006/jsvi.1999.2791.

Luciano, R., Darban, H., Bartolomeo, Fabbrocino, F., Scorza, D. (2020), "Free flexural vibrations of nanobeams with non-classical boundary conditions using stress-driven nonlocal model", *Mech. Res. Commun.*, **107**, 103536. https://doi.org/10.1016/j.mechrescom.2020.103536.

Madan, R. and Bhowmick, S. (2020), "A review on application of FGM fabricated using solid-state processes", *Adv. Mater. Proc. Technol.*, **6**(3), 608-619. https://doi.org/10.1080/2374068X.2020.1731153.

Madan, R. and Bhowmick, S. (2022), "Fabrication and micro-structural characterization of Al-SiC based functionally graded disk", *Aircr. Eng. Aerosp. Technol.*, **95**(2), 292-301. https://doi.org/10.1108/AEAT-03-2022-0096.

Mahi, A., Adda Bedia, E.A. and Tounsi, A. (2015), "A new hyperbolic shear deformation theory for bending and free vibration analysis of isotropic, functionally graded, sandwich and laminated composite plates", *Appl. Math. Modell.*, **39**(9), 2489-2508. https://doi.org/10.1016/j.apm.2014.10.045.

Menasria, A., Kaci, A., Bousahla, A.A., Bourada, F., Tounsi, A., Benrahou, K.H., Tounsi, A., Adda Bedia, E.A. and Mahmoud, S.R. (2020), "A four-unknown refined plate theory for dynamic analysis of FG-sandwich plates under various boundary conditions", *Steel Compos. Struct.*, **36**(3), 355-367. https://doi.org/10.12989/SCS.2020.36.3.355.

Mirjavadi, S.S., Forsat, M., Hamouda, A. and Barati, M.R. (2019), "Dynamic response of functionally graded graphene nanoplatelet reinforced shells with porosity distributions under transverse dynamic loads", *Mater. Res. Exp.*, **6**(7), 075045. https://doi.org/10.1088/2053-1591/ab1552.

Mohd, F. and Talha, M. (2022), "Effect of graphene platelets reinforcement on vibration behavior of functionally graded porous arches under thermal environment", *Mater. Today Proc.*, **61**, 103-109. https://doi.org/10.1016/j.matpr.2022.03.663.

Muni Rami Reddy, R., Karunasena, W. and Lokuge, W. (2018), "Free vibration of functionally graded-GPL reinforced composite plates with different boundary conditions", *Aerosp. Sci. Technol.*, **78**, 147-156. https://doi.org/10.1016/j.ast.2018.04.019.

Nakamura, T., Wang, T. and Sampath, S. (2000), "Determination of properties of graded materials by inverse analysis and instrumented indentation", *Acta Materialia*, **48**(17), 4293-4306.

https://doi.org/10.1016/S1359-6454(00)00217-2.
Norio, H., Hideaki, I. and Takuji, N. (1992), "Stress intensity factors of cracks initiating from a rhombic hole due to uniform heat flux", *Eng. Fract. Mech.*, **42**(2), 331-337. https://doi.org/10.1016/0013-7944(92)90223-2.
Nebab, M., Dahmane, M., Ayache, B., Ait Atmane, H., Bernard, F., Benadouda, M., Bennai, R., Hadji, L. (2023), "Fundamental frequencies of cracked FGM beams with influence of porosity and Winkler/Pasternak/Kerr foundation support using a new quasi-3D HSDT", *Mech. Adv. Mater. Struct.*, 1-13. https://doi.org/10.1080/15376494.2023.2294371.
Phung-Van, P., Lieu, Q.X., Ferreira, A.J.M. and Thai, C.H. (2021), "A refined nonlocal isogeometric model for multilayer functionally graded graphene platelet-reinforced composite nanoplates", *Thin Wall. Struct.*, **164**, 107862. https://doi.org/10.1016/j.tws.2021.107862.
Sankar, B.V. (2001), "An elasticity solution for functionally graded beams", *Compos. Sci. Technol.*, **61**(5), 689-696. https://doi.org/10.1016/S0266-3538(01)00007-0.
Shimpi, R.P. (2002), "Refined plate theory and its variants", *AIAA J.*, **40**(1), 137-146. https://doi.org/10.2514/2.1622
Sobhy, M. (2013), "Buckling and free vibration of exponentially graded sandwich plates resting on elastic foundations under various boundary conditions", *Compos. Struct.*, **99**, 76-87. https://doi.org/10.1016/j.compstruct.2012.11.018.
Song, M., Yang, J., Kitipornchai, S. and Zhu, W. (2017), "Buckling and postbuckling of biaxially compressed functionally graded multilayer graphene nanoplatelet-reinforced polymer composite plates", *Int. J. Mech. Sci.*, **131-132**, 345-355. https://doi.org/10.1016/j.ijmecsci.2017.07.017.
Taibi, F.Z., Benyoucef, S., Tounsi, A., Bachir Bouiadjra, R., Adda Bedia, E.A. and Mahmoud, S. (2015), "A simple shear deformation theory for thermo-mechanical behaviour of functionally graded sandwich plates on elastic foundations", *J. Sandw. Struct. Mater.*, **17**(2), 99-129. https://doi.org/10.1177/1099636214554904.
Tavakol, M.R., Tooski, M.Y., Jabbari, M. and Javadi, M. (2023), "Experimental and numerical investigation of the effect of graphene nanoparticles on the strength of sandwich structures under low-velocity impact", *Funct. Compos. Struct.*, **5**(1), 015002. https://doi.org/10.1088/2631-6331/acb88f.
Thai, C.H., Ferreira, A.J.M., Tran, T.D. and Phung-Van, P. (2019), "Free vibration, buckling and bending analyses of multilayer functionally graded graphene nanoplatelets reinforced composite plates using the NURBS formulation", *Compos. Struct.*, **220**, 749-759. https://doi.org/10.1016/j.compstruct.2019.03.100.
Twinkle, C.M. and Pitchaimani, J. (2021), "Free vibration and stability of graphene platelet reinforced porous nano-composite cylindrical panel: Influence of grading, porosity and non-uniform edge loads", *Eng. Struct.*, **230**, 111670. https://doi.org/10.1016/j.engstruct.2020.111670.
Yang, J., Wu, H. and Kitipornchai, S. (2017), "Buckling and postbuckling of functionally graded multilayer graphene platelet-reinforced composite beams", *Compos. Struct.*, **161**, 111-118. https://doi.org/10.1016/j.compstruct.2016.11.048.
Zouatnia, N., Hadji, L., Atmane, H.A., Nebab, M., Madan, R., Bennai, R. and Dahmane, M. (2024), "Analysis of free vibration in bi-directional power law-based FG beams employing RSD theory", *Coupl. Syst. Mech.*, **13**(4), 359-373. https://doi.org/10.12989/CSM.2024.13.4.359.